



# Macrophages promote network formation and maturation of transplanted adipose tissue–derived microvascular fragments

Thomas Später<sup>1</sup> , Maximilian M Menger<sup>1,2</sup>, Ruth M Nickels<sup>1</sup>, Michael D Menger<sup>1</sup> and Matthias W Laschke<sup>1</sup> 

## Abstract

Adipose tissue–derived microvascular fragments rapidly reassemble into microvascular networks within implanted scaffolds. Herein, we analyzed the contribution of macrophages to this process. C57BL/6 mice received clodronate (clo)-containing liposomes for macrophage depletion, whereas animals treated with phosphate-buffered-saline-containing liposomes served as controls. Microvascular fragments were isolated from clo- and phosphate-buffered-saline-treated donor mice and seeded onto collagen–glycosaminoglycan matrices, which were implanted into dorsal skinfold chambers of clo- and phosphate-buffered-saline-treated recipient mice. The implants' vascularization and incorporation were analyzed by stereomicroscopy, intravital fluorescence microscopy, histology, and immunohistochemistry. Compared to controls, matrices within clo-treated animals exhibited a significantly reduced functional microvessel density. Moreover, they contained a lower fraction of microvessels with an  $\alpha$ -smooth muscle actin (SMA)<sup>+</sup> cell layer, indicating impaired vessel maturation. This was associated with a deteriorated implant incorporation. These findings demonstrate that macrophages not only promote the reassembly of microvascular fragments into microvascular networks, but also improve their maturation during this process.

## Keywords

Tissue engineering, microvascular fragments, scaffold, vascularization, clodronate, macrophage depletion, immune cells

Received: 6 January 2020; accepted: 18 February 2020

## Introduction

The establishment of an effective vascular supply represents a key challenge to ensure a successful incorporation and long-term function of implanted tissue constructs.<sup>1</sup> This can be achieved by the seeding of scaffolds with endothelial progenitor cells,<sup>2</sup> mesenchymal stem cells,<sup>3,4</sup> keratinocytes,<sup>5,6</sup> glandular-derived stem cells,<sup>7</sup> dermal fibroblasts,<sup>6</sup> or induced pluripotent stem cell–derived endothelial cells.<sup>8</sup> Of interest, the prevascularization of scaffolds with adipose tissue–derived microvascular fragments (MVF) has recently been described to be even superior when compared to such single cell–based approaches.<sup>9</sup>

MVFs bear the major advantage that they can be easily isolated from adipose tissue in large amounts.<sup>10</sup> Unlike single cells, MVFs represent biologically intact blood vessel segments that rapidly interconnect with each other as well as with the surrounding host microvasculature, leading to

the formation of new blood-perfused networks within implanted scaffolds.<sup>2,11</sup> Accordingly, it may be speculated that in future clinical practice MVFs serve as autologous vascularization units, which are harvested intraoperatively from fat samples and retransferred during the ongoing procedure into a tissue defect of the same patient.

Of note, the course of the early inflammatory host tissue response to implanted biomaterials crucially contributes to their degree of vascularization and incorporation.<sup>12</sup>

<sup>1</sup>Institute for Clinical & Experimental Surgery, Saarland University, Homburg, Germany

<sup>2</sup>Department of Trauma, Hand and Reconstructive Surgery, Saarland University, Homburg, Germany

### Corresponding author:

Thomas Später, Institute for Clinical & Experimental Surgery, Saarland University, Kirrberger Straße; Geb. 65/66, 66421 Homburg, Saarland, Germany.

Email: thomas.spaeter@uks.eu



During this process, several angiogenic growth factors, such as vascular endothelial growth factor (VEGF) or basic fibroblast growth factor (bFGF), are released by macrophages, particularly of the M2 phenotype.<sup>13,14</sup> In fact, after their recruitment from the blood stream toward the site of biomaterial implantation, macrophages not only act as phagocytes to clear cellular debris, but also as a major source of pro-angiogenic cytokines and growth factors.<sup>15,16</sup>

In a previous study, we have already shown that MVF-prevascularized collagen–glycosaminoglycan matrices contain significant numbers of CD68<sup>+</sup> macrophages after their implantation.<sup>17</sup> However, the influence of these immune cells on the network forming capacity of MVFs has not been analyzed so far. Based on the crucial role of macrophages in angiogenesis, we herein hypothesized that they promote the interconnection of MVFs with each other and, thus, the vascularization and incorporation of MVF-seeded scaffolds.

To test this hypothesis, we used dichloromethylene bisphosphonate (clodronate (clo)) encapsulated in liposomes to induce apoptosis of macrophages in C57BL/6 mice, whereas phosphate-buffered saline (PBS)-containing liposomes served as controls. MVFs were isolated from the epididymal fat pads of clo- or PBS-treated donor mice and subsequently seeded onto collagen–glycosaminoglycan matrices. In previous studies, we found that MVFs seeded onto these matrices, which are frequently used as dermal substitutes in clinical practice, exhibit a high viability and rapidly invade their porous matrix structure to form new microvascular networks.<sup>9,10,17</sup> The seeded matrices were implanted into full-thickness skin defects within dorsal skinfold chambers of clo- or PBS-treated recipient animals. The vascularization and incorporation of the implants were analyzed by means of intravital fluorescence microscopy throughout 14 days as well as histology and immunohistochemistry at the end of the 14 days observation period.

## Materials and methods

### Animals

All animal experiments were approved by the local governmental animal protection committee (permit number: 48/2018) and conducted in accordance with the European legislation on the protection of animals (Directive 2010/63/EU) and the NIH Guidelines on the Care and Use of Laboratory Animals (NIH publication #85-23 Rev. 1985).

Dorsal skinfold chambers were implanted in C57BL/6 wild-type mice (Institute for Clinical & Experimental Surgery, Saarland University, Homburg/Saar, Germany) with an age of 3–6 months and a body weight of 24–30 g. Epididymal fat was isolated from green fluorescent protein (GFP)<sup>+</sup> donor mice (C57BL/6-Tg(CAG-EGFP)10sb/J; The Jackson Laboratory, Bar Harbor, ME, United States)

with an age of 7–12 months and a body weight of >30 g. The animals were housed under a 12-h day/night cycle and were fed with water and standard pellet food (Altromin, Lage, Germany) ad libitum.

### Isolation of MVFs

As previously described in detail, MVFs (Figure 1(a)) were harvested from the epididymal fat pads of GFP<sup>+</sup> C57BL/6 donor mice.<sup>18</sup> Briefly, collagenase NB4G (0.5 U/mL; Serva, Heidelberg, Germany) was used to enzymatically digest the fat tissue under slight stirring and humidified atmospheric conditions (37°C, 5% CO<sub>2</sub>) for ~10 min. The enzyme was then neutralized by adding two volumes of PBS supplemented with 20% fetal calf serum (FCS). After incubation of the suspension containing MVFs and single cells for 5 min at 37°C, the fat supernatant was removed and the remaining suspension was filtered through a 200- $\mu$ m mesh. Subsequently, the MVF-single cell suspension was enriched to a pellet by a 5-min centrifugation at 120 $\times$ g, which was then resuspended in 0.9% NaCl for the seeding of collagen–glycosaminoglycan matrices.

### Seeding of collagen–glycosaminoglycan matrices

To generate standardized collagen–glycosaminoglycan matrices for the experiments, 12.5-mm<sup>2</sup> samples were identically cut out of a 1.3 mm thick Integra<sup>®</sup> Dermal Regeneration Template Single Layer without silicone sheet (Integra Life Sciences, Ratingen, Germany) with a 4-mm biopsy punch (kai Europe GmbH, Solingen, Germany) and stored in PBS until their use. Before the seeding, 10  $\mu$ L PBS was carefully sucked out of the matrices by means of a pipette (Eppendorf, Wesseling-Berzdorf, Germany). They were then placed on a 500- $\mu$ m cell strainer, and 10  $\mu$ L 0.9% NaCl containing ~10,000 MVF and ~200,000 single cells were transferred onto the matrices (Figure 1(b)).<sup>9</sup> In addition, a 10- $\mu$ L pipette was used to induce negative pressure from underneath the matrices. In previous studies, we have already shown that this procedure results in a sufficient entrapment of MVFs within the superficial layers of the matrices, which is necessary to guarantee a rapid reassembly of individual MVFs into new microvascular networks.<sup>10,19</sup>

### Modified dorsal skinfold chamber model

MVF-seeded collagen–glycosaminoglycan matrices were implanted into full-thickness skin defects within dorsal skinfold chambers of C57BL/6 recipient mice (Figure 1(c)). For the implantation of the dorsal skinfold chamber (Irola Industriekomponenten GmbH & Co. KG, Schonach, Germany), the mice were anesthetized by an intraperitoneal injection of ketamine (75 mg/kg body weight);

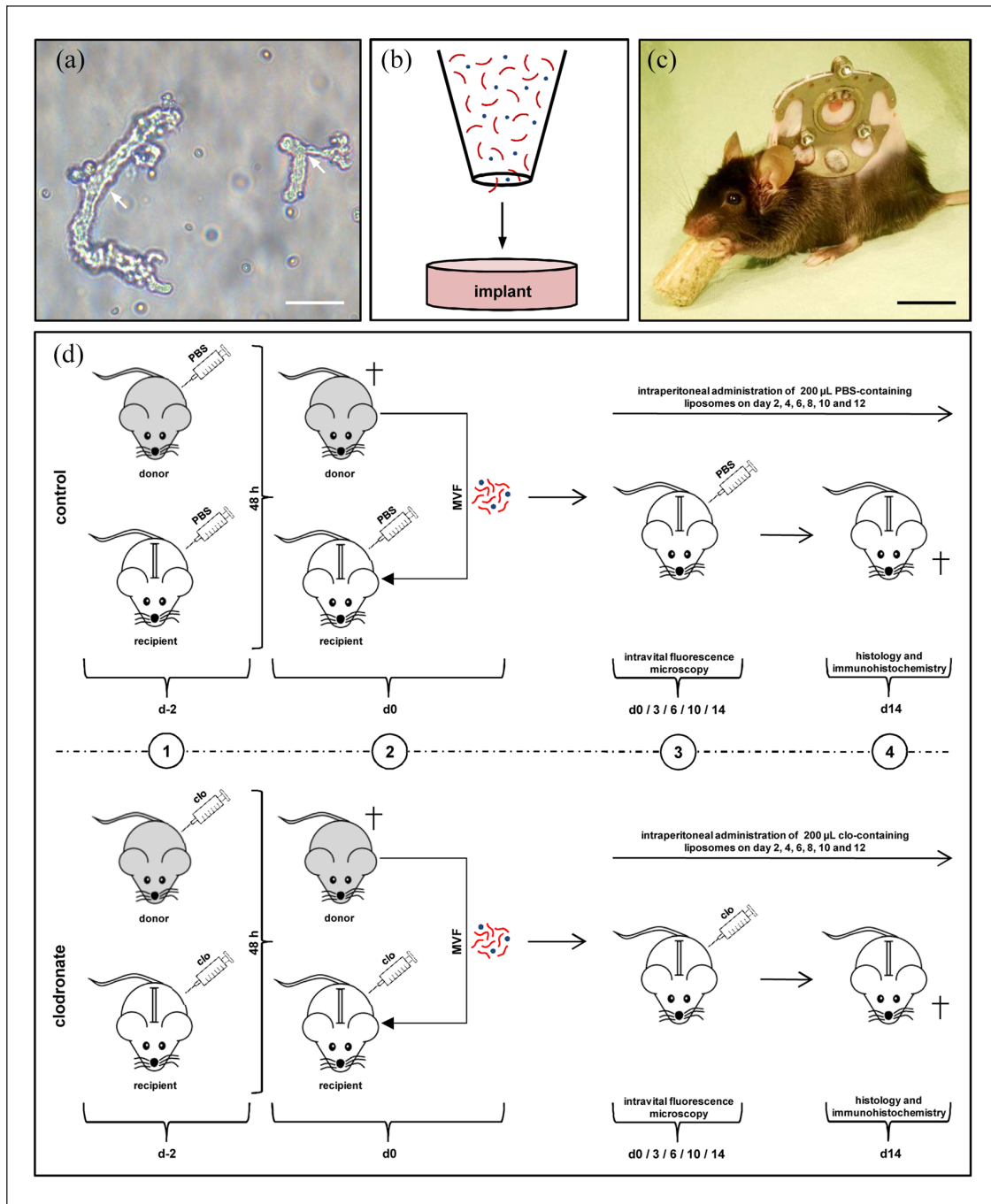


**Figure 1.** Model and experimental study design. (a) Freshly isolated MVFs (arrows) from the epididymal fat pads of a GFP<sup>+</sup> donor mouse. Scale bar: 40 μm. (b) Schematic illustration of collagen-glycosaminoglycan matrix seeding with MVFs (red) and single cells (blue). (c) C57BL/6 mouse with a dorsal skinfold chamber containing a full-thickness skin defect. Scale bar: 17.5 mm. (d) Schematic overview of the experimental protocol of the present study. 1: GFP<sup>+</sup> donor mice and GFP<sup>-</sup> recipient mice were treated with liposomes containing clo or PBS 48 h prior to MVF isolation (day -2). 2: MVFs were harvested from the epididymal fat pads of the donor animals, seeded onto collagen-glycosaminoglycan matrices and implanted into full-thickness skin defects within dorsal skinfold chambers of GFP<sup>-</sup> recipient mice, which were again treated with clo- and PBS-containing liposomes. 3: The recipient animals further received intraperitoneal injections of clo or PBS on days 2, 4, 6, 8, 10, and 12. The implants were microscopically analyzed on day 0, 3, 6, 10, and 14. 4: At the end of the 2-week observation period, the dorsal skinfold chamber preparations were processed for further histological and immunohistochemical analyses.

Ursotamin<sup>®</sup>; Serumwerk Bernburg, Bernburg, Germany) and xylazine (25 mg/kg body weight; Rompun<sup>®</sup>; Bayer, Leverkusen, Germany). For pain medication, all animals

received a subcutaneous injection of 5 mg/kg carprofen (Rimadyl<sup>®</sup>; Zoetis Deutschland GmbH, Berlin, Germany). Subsequently, the two symmetrical titanium frames of the

chamber were fixed on the extended dorsal skinfold. The animals were then allowed to recover for 48 h before a 4 mm in diameter full-thickness skin defect was created within the observation window of the chamber by means of a dermal biopsy punch (kai Europe GmbH). Each defect was then filled with a MVF-seeded collagen–glycosaminoglycan matrix, and the observation window was sealed again with a removable cover glass.

### Macrophage depletion

For macrophage depletion, we used clo-containing liposomes. To mimic an autologous transplantation of MVFs in the present study, as envisaged for their future clinical application, both donor and recipient mice received an intraperitoneal injection of 200  $\mu$ L clo- (5 mg/mL) or PBS-containing liposomes 48 h prior to the harvesting of MVFs and the implantation of MVF-seeded collagen–glycosaminoglycan matrices (Figure 1(d)). This dose has previously been used in other studies to successfully deplete macrophages.<sup>20,21</sup> In recipient animals, the treatment was repeated on day 0, that is, the day of matrix implantation, as well as on days 2, 4, 6, 8, 10, and 12 (Figure 1(d)).

### Stereomicroscopy

The epithelialization and hemorrhage formation of collagen–glycosaminoglycan matrices were assessed stereomicroscopically by means of repetitive planimetry. For this purpose, the anesthetized animals were fixed on a Plexiglas stage and the dorsal skinfold chamber was positioned under a stereomicroscope (Leica M651, Wetzlar, Germany) on day 0 (day of implantation), 3, 6, 10, and 14. To identify epithelialized and non-epithelialized areas, the chamber tissue was visualized in epi-illumination. Transillumination was further used to evaluate the extent of bleeding (given in % of implant surface) induced by the MVF-seeded matrices by means of a semiquantitative hemorrhagic score as follows - 1: no bleeding, 2: 1%–25%, 3: 26%–50%, 4: 51%–75%, 5: 76%–100% of the implant surface with bleeding, and 6: bleeding exceeding the implant surface.<sup>22</sup> All microscopic images were recorded by a DVD system and analyzed with the computer-assisted off-line analysis system CapImage (Version 8.5, Zeintl, Heidelberg, Germany). The epithelialized area (given in %) was calculated by the equation as follows: (total implant area – non-epithelialized implant area)/(total implant area)  $\times$  100.

### Intravital fluorescence microscopy

After stereomicroscopic analysis of the implants, 0.1 mL of the blood plasma marker 5% fluorescein isothiocyanate (FITC)-labeled dextran (150,000 Da; Sigma-Aldrich, Taufkirchen, Germany) was injected into the retrobulbar

venous plexus of the anesthetized animals for contrast enhancement. The chamber window was then positioned under a Zeiss Axiotech fluorescent epi-illumination microscope (Zeiss, Oberkochen, Germany) and microscopic images were recorded with a charge-coupled device video camera (FK6990; Pieper, Schwerte, Germany) and a DVD system for off-line analyses using CapImage (Zeintl). Throughout the entire observation period, the vascularization within the implants was assessed in 12 identical regions of interest (ROIs), which were determined before the experiment along a horizontal (6 ROIs) and vertical line (6 ROIs), covering the entire implant diameter. This enabled the repetitive assessment of the newly developing microvascular networks within each area over time. ROIs exhibiting red blood cell (RBC)-perfused microvessels were defined as perfused ROIs (given in % of all observed ROIs). Furthermore, the functional microvessel density was determined as the total length of all RBC-perfused microvessels per ROI ( $\text{cm}/\text{cm}^2$ ). In addition, the diameter ( $d$ ,  $\mu\text{m}$ ) and the centerline RBC velocity ( $v$ ,  $\mu\text{m}/\text{s}$ ) of 40 randomly selected microvessels were measured. These microhemodynamic parameters were used to calculate the wall shear rate ( $\dot{\gamma}$ ,  $\text{s}^{-1}$ ) by means of the Newtonian definition  $\dot{\gamma} = 8 \times v/d$ .

### Flow cytometry

To confirm the depletion efficiency of the injected liposomes, blood of PBS-treated ( $n=8$ ) and clo-treated ( $n=8$ ) mice was analyzed by means of flow cytometry at the end of the 2-week observation period. For this purpose,  $\sim 800 \mu\text{L}$  whole blood of the mice was collected in ethylenediaminetetraacetic acid (EDTA) tubes (Sarstedt, Nümbrecht, Germany). Subsequently, each blood sample was lysed with Pharm Lyse<sup>®</sup> (Becton Dickinson (BD), Heidelberg, Germany) for 30 min and washed twice with 20 mL PBS. Forward and side scatters were used to determine the percentage of monocytes within 10,000 leukocytic cells (granulocytes, monocytes, and lymphocytes) by means of a FACScan (BD Biosciences) and the software package CellQuest Pro (BD Biosciences).

### Histology and immunohistochemistry

Formalin-fixed samples of the dorsal skinfold preparation as well as the spleen and liver of recipient animals were embedded in paraffin and cut into 3- $\mu\text{m}$ -thick sections. According to standard procedures, hematoxylin and eosin (HE) staining of individual sections was performed. By means of a BX60 microscope (Olympus, Hamburg, Germany) and the imaging software cellSens Dimension 1.11 (Olympus), the density of infiltrating cells ( $\text{mm}^{-2}$ ) was assessed in 4 ROIs within the border (2 ROIs) and center (2 ROIs) zones of implanted MVF-seeded collagen–glycosaminoglycan matrices. To further quantify the

collagen content within the implants, additional sections were stained with Sirius red. The collagen content of the implants was also assessed in 4 ROIs within their border (2 ROIs) and center (2 ROIs) zones in relation to normal skin.<sup>10</sup>

Furthermore, sections were co-stained with a monoclonal rat anti-mouse antibody against the endothelial cell marker CD31 (1:100; Dianova, Hamburg, Germany) and a polyclonal goat antibody against GFP (1:200; Rockland Immunochemicals, Limerick, PA, United States), followed by a goat anti-rat IgG Alexa555 antibody (Life Technologies, Ober-Olm, Germany) and a biotinylated donkey anti-goat antibody (1:30; Dianova) as secondary antibodies. The biotinylated antibody was detected by streptavidin-Alexa488 (1:50; Life Technologies). Cell nuclei were stained with Hoechst 33342 (2 µg/mL; Sigma-Aldrich). The density of CD31<sup>+</sup> microvessels (mm<sup>-2</sup>) and the fraction of CD31<sup>+</sup>/GFP<sup>+</sup> microvessels (%) were quantitatively analyzed within the implants.

Additional sections were co-stained with a monoclonal rat anti-mouse antibody against CD31 (1:100; Dianova GmbH) and a rabbit anti-mouse antibody against  $\alpha$ -smooth muscle actin (SMA) (Abcam, Cambridge, United Kingdom) as primary antibodies. A goat anti-rat IgG Alexa555 antibody and a goat anti-rabbit Alexa488 antibody (1:100, Life Technologies) served as secondary antibodies. Cell nuclei on each section were stained with Hoechst 33342 (2 µg/mL; Sigma-Aldrich). On each section, 100 randomly selected microvessels within the implants were analyzed to assess the fraction of mature CD31<sup>+</sup>/SMA<sup>+</sup> microvessels (%).

For the immunohistochemical detection of CD68<sup>+</sup> macrophages as well as M1 and M2 macrophages, sections were incubated with a rabbit polyclonal anti-CD68 antibody (1:300; Abcam), a rabbit polyclonal anti-inducible nitric oxide synthase (iNOS) antibody (1:100; Abcam), and a rabbit polyclonal anti-CD163 antibody (1:200; Abcam) as primary antibodies, followed by a biotinylated goat anti-rabbit IgG antibody (ready-to-use; Abcam) or a goat anti-rabbit peroxidase antibody (ready-to-use; Abcam) as secondary antibodies. The biotinylated antibody was detected by peroxidase-labeled-streptavidin (ready-to-use; Abcam). The chromogen used was 3-amino-9-ethylcarbazole (Abcam). All sections were counterstained with Mayer's hemalum (Merck). To detect mast cells within the implants, additional sections were stained with toluidine blue according to standard protocols.<sup>23</sup>

For the immunohistochemical detection of the cytokerin<sup>+</sup> epithelial layer covering the implants on day 14, sections of the largest cross-sectional diameter of the matrices were incubated with a rabbit polyclonal anti-cytokeratin antibody (1:100; Abcam) as primary antibody, followed by a biotinylated goat anti-rabbit IgG antibody (ready-to-use; Abcam). The biotinylated antibody was detected by peroxidase-labeled-streptavidin (1:50; Sigma-Aldrich), and

3,3-diaminobenzidine (Sigma-Aldrich) was used as chromogen. Using a BZ-8000 microscopic system (Keyence, Osaka, Japan), the length of the cytokerin<sup>+</sup> epithelial layer and the diameter of the implants were measured to assess epithelialization as follows: (length of cytokerin<sup>+</sup> epithelial layer/total diameter of implant)  $\times$  100.

### Experimental protocol

MVFs were harvested from the epididymal fat pads of six GFP<sup>+</sup> donor mice. Three of the six animals were intraperitoneally injected with clo-containing liposomes 48 h prior to MVF isolation (Figure 1(d)). The other three animals received PBS-containing liposomes. Subsequently, the isolated MVFs were seeded onto collagen–glycosaminoglycan matrices (n=8 per group). These matrices were implanted into full-thickness skin defects within dorsal skinfold chambers of 16 GFP<sup>-</sup> C57BL/6 wild-type mice. Eight of these 16 mice already received an intraperitoneal injection of clo-containing liposomes on the day of dorsal skinfold chamber implantation. The other eight animals received PBS-containing liposomes. The treatment was repeated on day 0, that is, the day of matrix implantation, as well as on days 2, 4, 6, 8, 10, and 12 (Figure 1(d)). To mimic an autologous transplantation of MVFs under our experimental conditions, only clo-treated recipients received matrices seeded with MVFs from clo-treated donors and only PBS-treated recipients received matrices seeded with MVFs from PBS-treated donors. Vascularization, incorporation, epithelialization, and hemorrhage formation of the matrices were assessed by means of repetitive stereomicroscopy and intravital fluorescence microscopy on day 0, 3, 6, 10, and 14. At the end of the 14-day observation period, all animals were sacrificed by means of cervical dislocation in deep anesthesia and the dorsal skinfold chamber preparations were processed for histological and immunohistochemical analyses.

### Statistical analysis

After testing the data for normal distribution and equal variance, differences between the two groups were analyzed by the unpaired Student's t-test (SigmaPlot 11.0; Jandel Corporation, San Rafael, CA, United States). In case of non-parametric data, a Mann–Whitney rank sum test was used. All values are expressed as means  $\pm$  standard error of the mean (SEM). Statistical significance was accepted for a value of  $p < 0.05$ .

## Results

### Implant vascularization

The vascularization of MVF-seeded collagen–glycosaminoglycan matrices was repetitively analyzed within dorsal

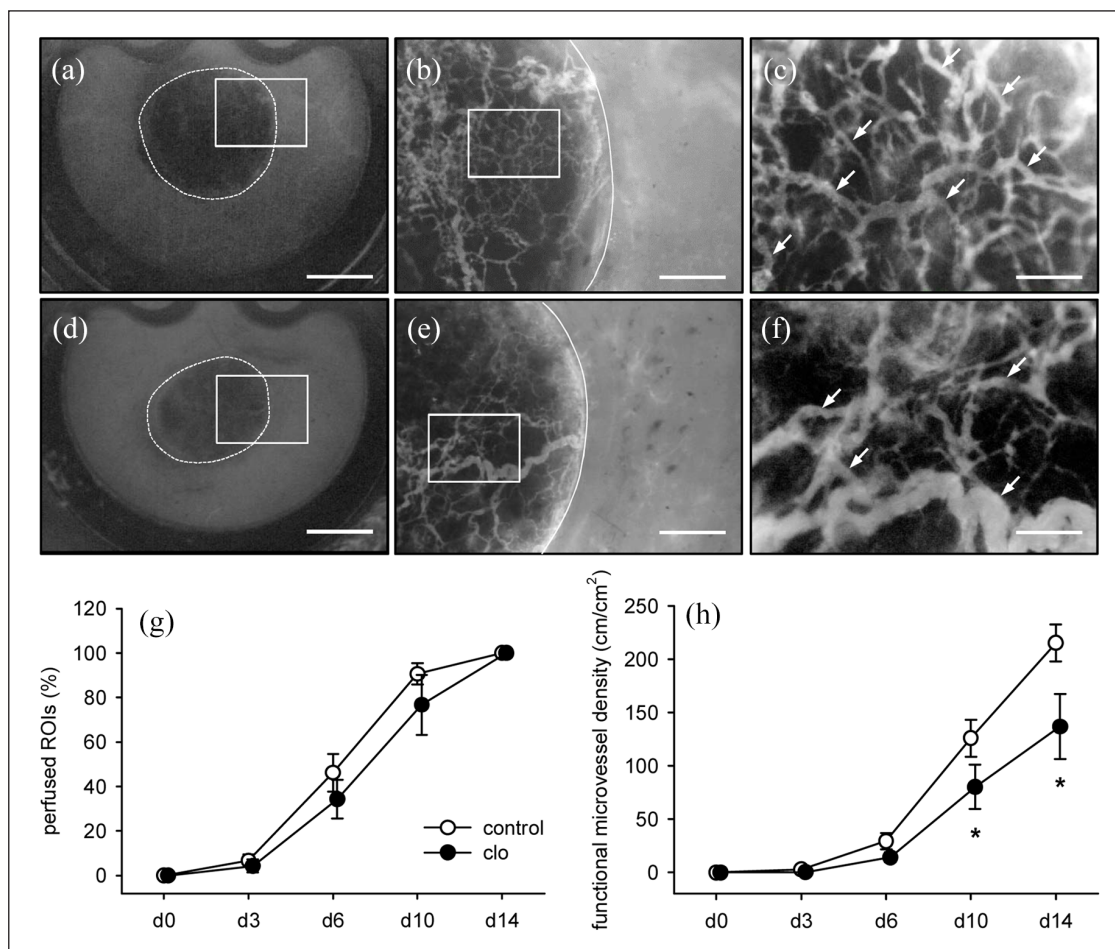


**Figure 2.** In vivo vascularization capacity of MVFs. (a–f) Intravital fluorescence microscopy (blue light epi-illumination, 5% FITC-labeled dextran intravenously) of MVF-seeded matrices on day 14 after implantation into full-thickness skin defects within dorsal skinfold chambers of PBS- (a–c) and clo-treated (d–f) C57BL/6 mice (a, d = overview of chamber observation window; b, e = higher magnification of inserts in a and d; c, f = higher magnification of inserts in b and e; broken lines = implant borders; arrows = perfused microvessels). Scale bars: a, d = 2.1 mm; b, e = 565  $\mu$ m; c, f = 150  $\mu$ m. (g, h) Perfused ROIs (g, %) and functional microvessel density (h,  $\text{cm}/\text{cm}^2$ ) of MVF-seeded matrices within dorsal skinfold chambers of PBS- (control; white circles;  $n=8$ ) and clo-treated (black circles;  $n=8$ ) mice. Means  $\pm$  SEM. \* $p < 0.05$  vs control.

skinfold chambers of clo- and PBS-treated mice by means of intravital fluorescence microscopy (Figure 2(a)–(f)). Throughout the 2-week observation period, the seeded MVFs reassembled into new microvascular networks within the implants and also developed interconnections with the microvasculature of the surrounding host tissue. The implants of both groups showed a comparable percentage of perfused ROIs over time (Figure 2(g)). However, the functional microvessel density within the matrices of clo-treated animals was significantly lower on days 10 and 14 after implantation when compared to controls (Figure 2(h)).

The process of matrix vascularization was characterized by decreasing vessel diameters as well as increasing centerline RBC velocities and wall shear rates of individual microvessels (Figure 3(a)–(e)). Of interest, the microvessels within implants of clo-treated animals exhibited a

significantly larger diameter when compared to controls (Figure 3(c)). In contrast, the centerline RBC velocity within these vessels was reduced (Figure 3(d)), resulting in a significantly lower wall shear rate (Figure 3(e)).

### Implant-induced bleeding

To assess implant-induced hemorrhage formation, the implanted collagen–glycosaminoglycan matrices were further analyzed by means of trans-illumination stereomicroscopy (Figure 4(a)–(f)). The highest hemorrhagic scores for both clo- and PBS-treated matrices were detected on day 6 after implantation (Figure 4(g)). The extent of hemorrhage formation did not differ between the two groups throughout the entire observation period.

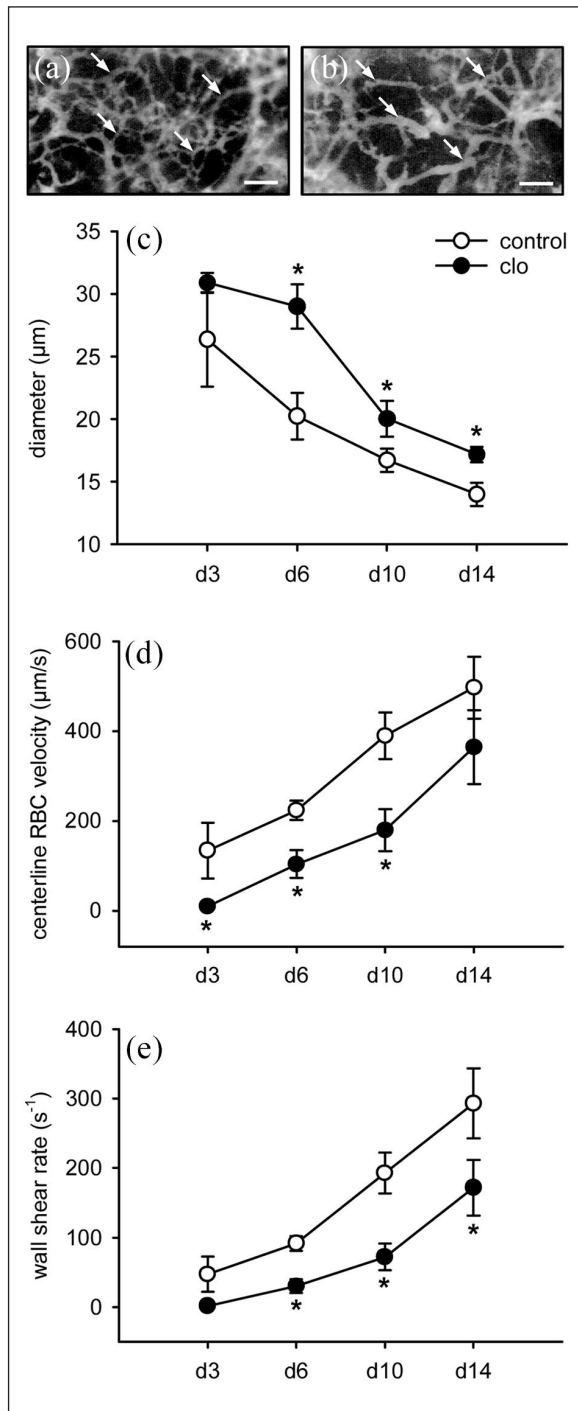


**Figure 3.** Microhemodynamics of newly developing microvascular networks. (a, b) Intravital fluorescence microscopy (blue light epi-illumination, 5% FITC-labeled dextran intravenously) of microvessels (arrows) within MVF-seeded matrices on day 14 after implantation into full-thickness skin defects in the dorsal skinfold chamber of a PBS- (a) and a clo-treated (b) C57BL/6 mouse. Scale bars: 80 μm. (c–e) Diameter (c, μm), centerline RBC velocity (d, μm/s), and wall shear rate (e, s<sup>-1</sup>) of individual microvessels within MVF-seeded matrices in dorsal skinfold chambers of PBS- (control; white circles; n=8) and clo-treated (black circles; n=8) mice. Means ± SEM. \*p < 0.05 vs control.

### Implant incorporation

At the end of the in vivo experiments, additional histological and immunohistochemical analyses were performed to study the incorporation of the MVF-seeded matrices. HE-stained sections revealed a lower amount of granulation tissue within clo-treated implants, as indicated by a significantly reduced number of infiltrating cells ( $4011 \pm 521$  cells/mm<sup>2</sup>) when compared to PBS-treated controls ( $5693 \pm 221$  cells/mm<sup>2</sup>;  $p < 0.05$ ) (Figure 5(a) and (b)). In line with this, these implants also contained markedly less mature collagen type I fibers, as assessed by polarized light microscopy of Sirius red-stained sections (Figure 5(c)–(f)). Furthermore, the density of CD31<sup>+</sup> microvessels was significantly reduced within the matrices of clo-treated animals (Figure 6(a)–(e)). In both groups, ~80% of all detected CD31<sup>+</sup> microvessels were also positive for GFP, proving their origin from the seeded MVFs (Figure 6(f)–(i)). Finally, the implants within clo-treated mice revealed a significantly reduced number of microvessels exhibiting a perivascular α-SMA<sup>+</sup> cell layer, indicating a lower maturation stage of the newly developed microvascular networks (Figure 6(j)–(l)).

### Immune cell infiltration of the implants

Flow cytometric analyses were performed to prove the successful macrophage depletion by clo-containing liposomes. These analyses revealed a significantly reduced number of circulating monocytes within the blood of clo-treated mice when compared to PBS-treated controls (Figure 7(a)–(c)). Moreover, the number of CD68<sup>+</sup> macrophages was significantly lower within the liver ( $57.6 \pm 5.4$  mm<sup>-2</sup>) and spleen ( $897.9 \pm 163.0$  mm<sup>-2</sup>) of clo-treated animals when compared to controls ( $199.4 \pm 33.8$  mm<sup>-2</sup> and  $1617.6 \pm 211.9$  mm<sup>-2</sup>, respectively). In line with these findings, the implants of clo-treated mice contained markedly less CD68<sup>+</sup> macrophages at the end of the 2-week observation period (Figure 7(d), (e), and (l)). Accordingly, they also presented with lower numbers of M1 and M2 macrophages as well as multi-nucleated giant cells (MNGCs) (Figure 7(f)–(k) and (m)–(o)). In contrast, the matrices of both groups exhibited a comparable number of infiltrating mast cells (Figure 7(p)–(r)).

### Implant epithelialization

The continuous access to the implanted matrices through the observation window of the dorsal skinfold chamber additionally allowed the repetitive stereomicroscopic analysis of implant epithelialization (Figure 8(a)–(d)). Although not proven to be significant, the matrices of clo-treated mice revealed a reduced epithelialization throughout the entire observation period when compared to PBS-treated controls (Figure 8(e)). This finding was

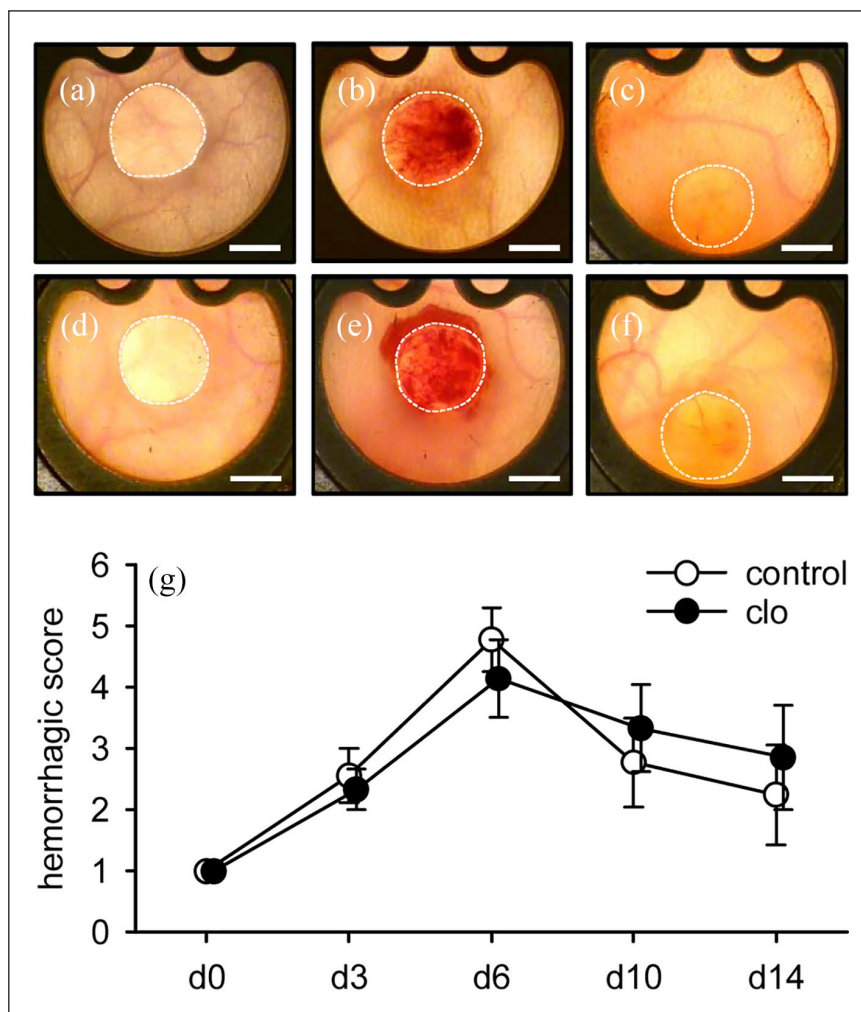


**Figure 4.** Implant-induced hemorrhage formation. (a–f) Trans-illumination stereomicroscopy of MVF-seeded matrices on day 0 (a, d), 6 (b, e), and 14 (c, f) after implantation into full-thickness skin defects within dorsal skinfold chambers of PBS- (a–c) and clo-treated (d–f) C57BL/6 mice. Scale bars: 2 mm. (g) Hemorrhagic score of MVF-seeded matrices within dorsal skinfold chambers of PBS- (control; white circles;  $n=8$ ) and clo-treated (black circles;  $n=8$ ) mice. Means  $\pm$  SEM.

confirmed by the immunohistochemical detection of the newly developing cytokeratin<sup>+</sup> epithelial layer, progressively covering the surface of the implants over time (Figure 8(f)–(h)).

## Discussion

In tissue engineering, MVFs represent promising building blocks, which have already been used in experimental studies for the vascularization of different scaffold biomaterials,<sup>10,19,24</sup> skin flaps,<sup>25,26</sup> superficial myocardium,<sup>27</sup> epicardial patches<sup>28</sup> as well as large bone and muscle defects.<sup>29–31</sup> Notably, the harvesting of MVFs from adipose tissue typically results in an isolate that includes various types of single cells, including adipocytes, mesenchymal stem cells, and immune cells.<sup>9,10</sup> On the other hand, implanted MVF-seeded scaffolds are rapidly infiltrated by immune cells, particularly macrophages, from the surrounding host tissue.<sup>32</sup> The present study now

demonstrates the crucial importance of these immune cells for the functionality of MVFs. In fact, we have shown that macrophages promote network formation and maturation of MVFs within collagen–glycosaminoglycan matrices, which were implanted into full-thickness skin defects.

We herein treated both MVF donor and recipient mice with clo-containing liposomes. Once ingested by macrophages, the phospholipid bilayers of these liposomes are disrupted under the influence of lysosomal phospholipases and the strongly hydrophilic clo molecules are intracellularly released.<sup>33</sup> As soon as a certain concentration of clo is reached, irreversible damage causes macrophages to undergo apoptosis.<sup>34–37</sup> This widely used method is considered the best approach to selectively deplete macrophages in mammals.<sup>37–39</sup> As demonstrated by Ferenbach et al.,<sup>40</sup> clo-induced macrophage depletion is typically associated with a reduced number of circulating monocytes. This finding was confirmed by our flow cytometric analyses. In



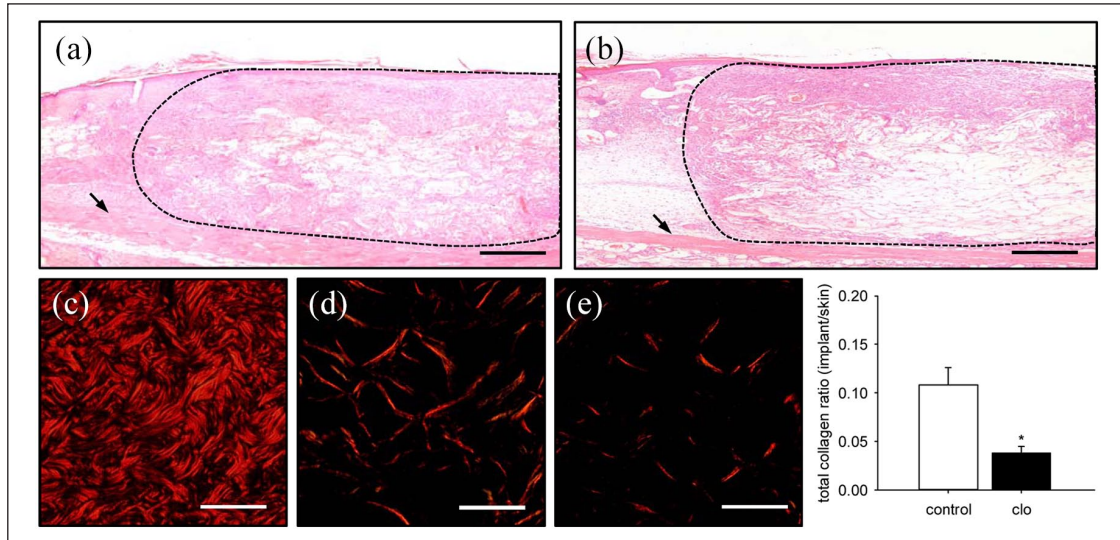


**Figure 5.** Final incorporation of MVF-seeded matrices. (a, b) HE-stained sections of MVF-seeded matrices on day 14 after implantation into full-thickness skin defects within the dorsal skinfold chamber of a PBS- (a) and a clo-treated (b) C57BL/6 mouse (broken lines = implant border; arrows = striated skin muscle). Scale bars: 260  $\mu$ m. (c–e) Polarized light microscopy of Sirius red-stained sections of normal skin (c) as well as MVF-seeded matrices of a PBS- (d) and a clo-treated (e) mouse. Scale bars: 50  $\mu$ m. (f) Total collagen ratio (implant/skin) within MVF-seeded matrices in PBS- (control; white bar; n = 8) and clo-treated (black bar; n = 8) mice. Means  $\pm$  SEM. \* $p < 0.05$  vs control.

addition, we detected a significantly lower number of CD68<sup>+</sup> macrophages within the implanted matrices as well as within the hepatic and splenic tissue of clo-treated animals when compared to controls. Accordingly, a markedly reduced number of MNGCs, which result from the fusion of individual macrophages,<sup>41</sup> was found within the implants of macrophage-depleted mice.

The effect of macrophage depletion on the vascularization capacity of MVFs was investigated in the dorsal skinfold chamber model. In combination with intravital fluorescence microscopy, this approach not only allows the repetitive analysis of microvascular network formation within implanted matrices, but also the assessment of the functionality of individual microvessels, as indicated by fluorescently labeled blood perfusion.<sup>1</sup> We found that MVF-seeded collagen–glycosaminoglycan matrices within dorsal skinfold chambers of clo- and PBS-treated animals exhibit a comparable percentage of perfused ROIs over time. However, the functional microvessel density within matrices of clo-treated mice was significantly lower when compared to controls. This reduced vascularization was further confirmed by immunohistochemical detection of CD31<sup>+</sup> microvessels within the implants at the end of the 2-week observation period. These results support the view that macrophages play an important role in the process of angiogenesis.<sup>42,43</sup> In fact, M2 macrophages are able to produce various pro-angiogenic factors, such as VEGF and bFGF.<sup>44,45</sup> Moreover, proteases secreted by macrophages contribute to the remodeling of the extracellular matrix and, thus, facilitate neovascularization.<sup>46</sup>

Finally, sophisticated studies indicate that macrophages can act as guides for endothelial tip cells and are involved in sprout anastomosis.<sup>47</sup> In the present study, macrophage depletion may have impaired all these mechanisms, resulting in reduced interconnections of individual MVFs and, thus, a lower density of the microvascular networks.

In addition, microvessels in clo-treated mice also showed a lack of maturation, as indicated by significantly larger vessel diameters as well as lower centerline RBC velocities and wall shear rates. Of note, macrophages produce transforming growth factor (TGF)- $\beta$ , a 25-kD homo- and heterodimer crucially involved in vascular development.<sup>48</sup> TGF- $\beta$  induces the expression of contractile proteins needed for vascular stabilization by eliciting the switch from mesenchymal stem cells toward the smooth muscle cell/pericyte lineage.<sup>49</sup> Furthermore, TGF- $\beta$  supports vessel stabilization through the stimulation of both migration and proliferation of smooth muscle cells.<sup>50,51</sup> In line with this knowledge, macrophage depletion resulted in a significantly reduced number of microvessels exhibiting a perivascular  $\alpha$ -SMA<sup>+</sup> cell layer within collagen–glycosaminoglycan matrices of clo-treated mice when compared to controls.

The development of new microvascular networks in MVF-seeded matrices is typically associated with hemorrhage formation.<sup>22</sup> This is particularly the case during the early phase of vascularization, when the interconnection of individual MVFs with each other and the surrounding host microvasculature is not yet fully completed. Accordingly, we detected the highest hemorrhagic score in both groups on day 6 after matrix implantation, corresponding to the

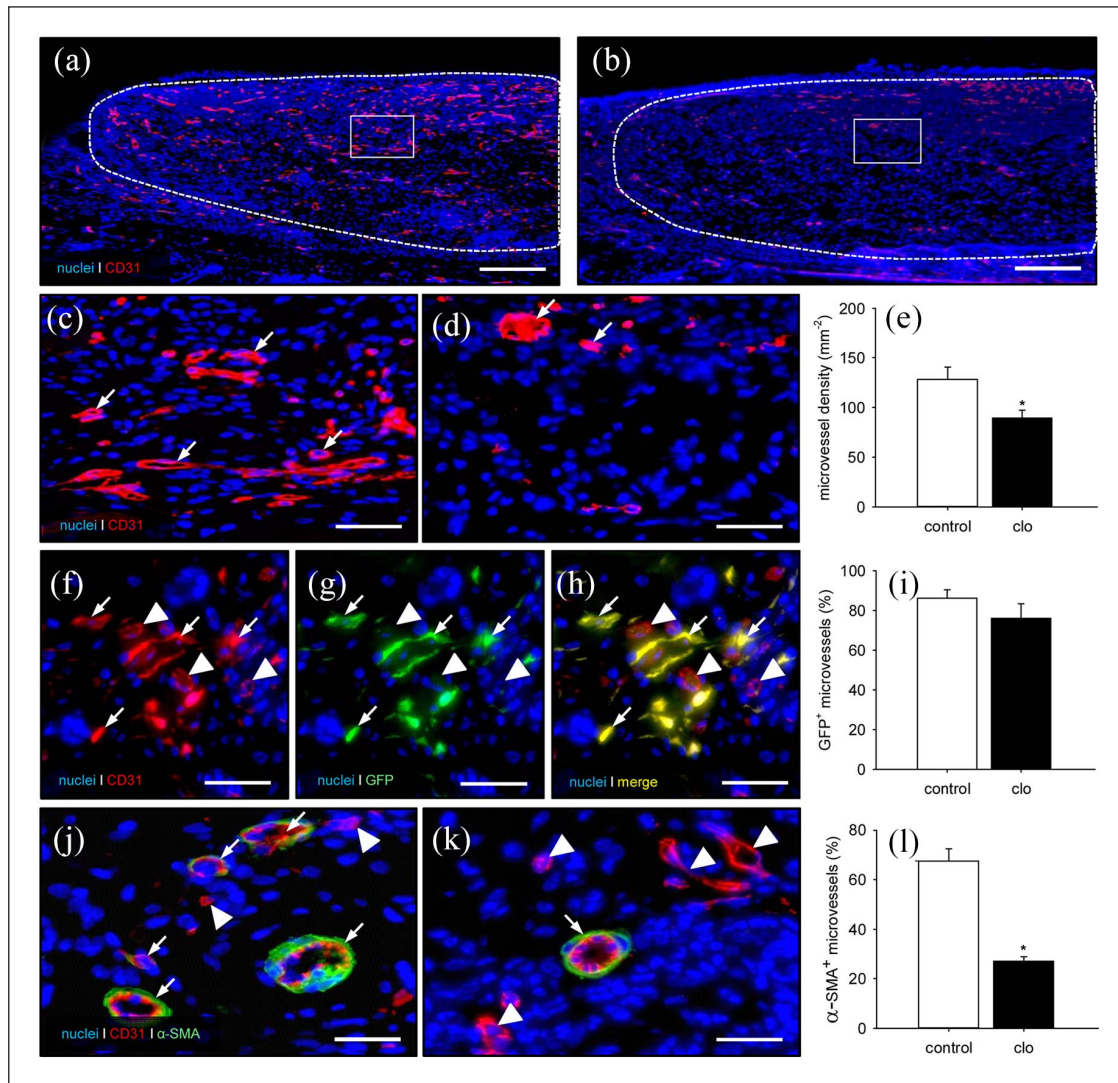


**Figure 6.** Final vascularization of MVF-seeded matrices. (a–d) Immunohistochemical detection of CD31<sup>+</sup> microvessels within MVF-seeded matrices in a PBS- (a, c) and a clo-treated (b, d) mouse (a, b = overview of the implants; c, d = higher magnification of inserts in a and b; broken lines = implant borders; arrows = CD31<sup>+</sup> microvessels). Scale bars: a, b = 230  $\mu$ m; c, d = 45  $\mu$ m. (e) Microvessel density ( $\text{mm}^{-2}$ ) within MVF-seeded matrices in PBS- (control; white bar; n = 8) and clo-treated (black bar; n = 8) mice. Means  $\pm$  SEM. \* $p < 0.05$  vs control. (f–h) Representative immunohistochemical detection of CD31<sup>+</sup>/GFP<sup>+</sup> microvessels (arrows) and CD31<sup>+</sup>/GFP<sup>-</sup> microvessels (arrowheads) within a MVF-seeded matrix of a clo-treated mouse. Scale bars: 30  $\mu$ m. (i) GFP<sup>+</sup> microvessels (%) within MVF-seeded matrices in PBS- (control; white bar; n = 8) and clo-treated (black bar; n = 8) mice. Means  $\pm$  SEM. (j, k) Immunohistochemical detection of CD31<sup>+</sup> microvessels with (arrows) and without (arrowheads) a perivascular  $\alpha$ -SMA<sup>+</sup> cell layer within MVF-seeded matrices of a PBS- (j) and a clo-treated (k) mouse. Scale bars: 18  $\mu$ m. (l)  $\alpha$ -SMA<sup>+</sup> microvessels (% of all blood vessels) within MVF-seeded matrices in PBS- (control; white bar; n = 8) and clo-treated (black bar; n = 8) mice. Means  $\pm$  SEM. \* $p < 0.05$  vs control.

onset of blood perfusion, as shown by intravital fluorescence microscopy. Of interest, we did not observe any significant differences in the extent of hemorrhage formation between the implants of clo- and PBS-treated mice throughout the entire observation period. This demonstrates that the implant-induced bleeding was not affected by the herein performed macrophage depletion.

To assess the incorporation of the MVF-seeded matrices, we additionally analyzed their epithelialization over

time and final collagen content on day 14 after implantation. Implants in clo-treated animals revealed a slightly reduced epithelialized surface throughout the entire observation period. This may be explained by a direct influence of macrophage-secreted TGF- $\beta$ . In fact, as previously described by Reynolds et al.,<sup>52</sup> elevated levels of TGF- $\beta$  lead to enhanced re-epithelialization of wounds. Moreover, we detected significantly less mature collagen type I fibers within matrices of clo-treated mice when compared to

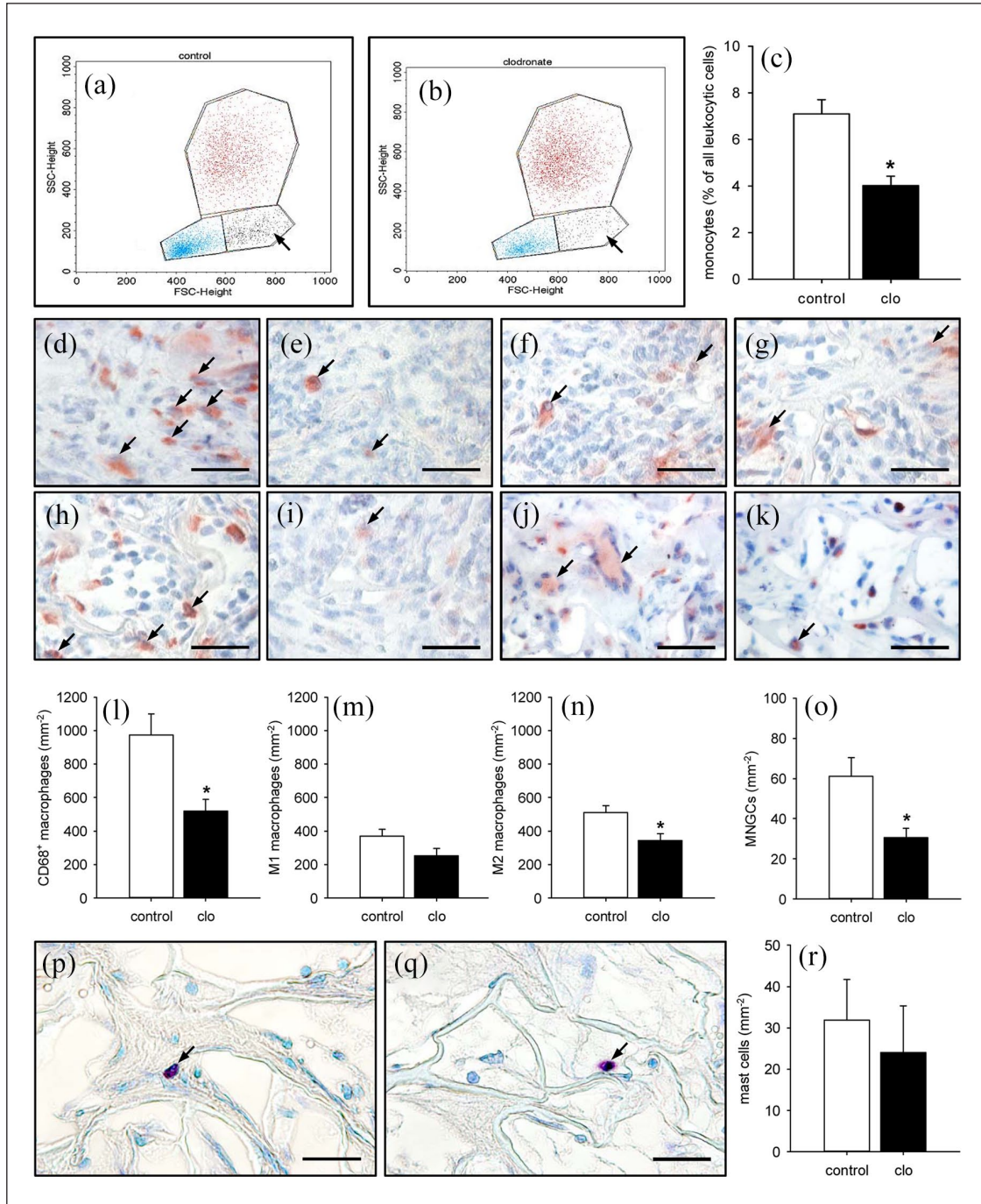


**Figure 7.** Systemic and implant-associated immune cells in PBS- and clo-treated animals. (a, b) Flow cytometric histograms showing the leukocyte population divided into lymphocytic (blue), monocytic (black; arrows), and granulocytic (red) subpopulations within lysed whole blood of PBS- (a) and clo-treated (b) C57BL/6 mice 14 days after matrix implantation. (c) Monocytes (% of all leukocytic cells) within the blood of PBS- (control; white bar; n=8) and clo-treated (black bar; n=8) mice. Means  $\pm$  SEM. \* $p < 0.05$  vs control. (d–k) Immunohistochemical detection of CD68<sup>+</sup> macrophages (d, e; arrows), M1 macrophages (f, g; arrows), M2 macrophages (h, i; arrows), and MNGCs (j, k; arrows) within MVF-seeded matrices of PBS- (d, f, h, j) and clo-treated (e, g, i, k) mice. Scale bars: 30  $\mu$ m. (l–o) CD68<sup>+</sup> macrophages (l; mm<sup>-2</sup>), M1 macrophages (m; mm<sup>-2</sup>), M2 macrophages (n; mm<sup>-2</sup>), and MNGCs (o; mm<sup>-2</sup>) within MVF-seeded matrices in PBS- (control; white bars; n=8) and clo-treated (black bars; n=8) mice. Means  $\pm$  SEM. \* $p < 0.05$  vs control. (p, q) Toluidine blue-stained sections showing mast cells (arrows) within MVF-seeded matrices of a PBS- (p) and a clo-treated (q) mouse. Scale bars: 30  $\mu$ m. (r) Mast cells (mm<sup>-2</sup>) within MVF-seeded matrices of PBS- (control; white bar; n=8) and clo-treated (black bar; n=8) mice. Means  $\pm$  SEM.

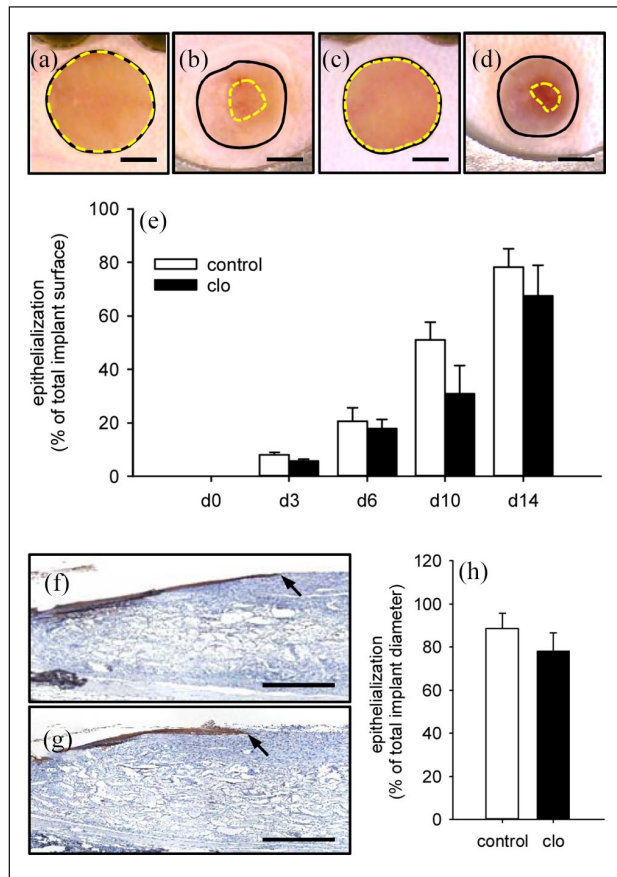


**Figure 8.** Implant epithelialization. (a–d) Stereomicroscopic images of MVF-seeded matrices on day 0 (a, c) and 14 (b, d) after implantation into full-thickness skin defects within dorsal skinfold chambers of a PBS- (a, b) and a clo-treated (c, d) C57BL/6 mouse (closed black lines = total implant areas; broken yellow lines = non-epithelialized implant areas). Scale bars: 1.3 mm. (e) Epithelialization (% of total implant surface) of MVF-seeded matrices within dorsal skinfold chambers of PBS- (control; white bars;  $n=8$ ) and clo-treated (black bars;  $n=8$ ) mice. Means  $\pm$  SEM. (f, g) Immunohistochemical detection of the cytokeratin<sup>+</sup> epithelial layer (arrows) covering MVF-seeded matrices in a PBS- (f) and a clo-treated (g) mouse. Scale bars: 500  $\mu$ m. (h) Epithelialization (% of total implant diameter) of MVF-seeded matrices within dorsal skinfold chambers of PBS- (control; white bar;  $n=8$ ) and clo-treated (black bar;  $n=8$ ) mice. Means  $\pm$  SEM.

controls. This may be due to the fact that macrophages are major players in collagen synthesis.<sup>53</sup> On the other hand, because adequate vascularization is a major prerequisite for implant incorporation,<sup>10</sup> the reduced collagen content may also be due to the impaired microvascular network formation within implants of macrophage-depleted animals.

## Conclusion

The present study demonstrates that macrophages crucially contribute to the vascularization capacity of MVFs. They do not only promote the reassembly of MVFs into

new microvascular networks, but also improve their maturation during this process. It should be noted that the numbers and activity of macrophages significantly differ between individual patients dependent on the status of their immune system.<sup>54,55</sup> Hence, our novel findings indicate that this may also determine the outcome of future clinical interventions using MVFs as vascularization units.

## Acknowledgements

The authors are grateful for the excellent technical assistance of Sandra Hans (Institute for Clinical & Experimental Surgery, Saarland University, Homburg/Saar, Germany).

## Availability of data and materials

All the data can be obtained in this manuscript.

## Declaration of conflicting interest

The author(s) declared no potential conflicts of interest with respect to the research, authorship, and/or publication of this article.

## Research ethics


This study was approved by the local governmental animal protection committee (Landesamt für Verbraucherschutz, Saarbrücken; permission number: 48/2018) and conducted in accordance with the Directive 2010/63/EU and the NIH Guidelines for the Care and Use of Laboratory Animals (NIH publication #85-23 Rev. 1985).

## Funding

The author(s) disclosed receipt of the following financial support for the research, authorship, and/or publication of this article: We acknowledge support by the Deutsche Forschungsgemeinschaft (DFG, German Research Foundation) and Saarland University within the funding program Open Access Publishing.

## ORCID iDs

Thomas Später  <https://orcid.org/0000-0002-1008-6376>

Matthias W Laschke  <https://orcid.org/0000-0002-7847-8456>

## References

- Laschke MW and Menger MD. Adipose tissue-derived microvascular fragments: natural vascularization units for regenerative medicine. *Trends Biotechnol* 2015; 33(8): 442–448.
- Hur J, Yoon CH, Kim HS, et al. Characterization of two types of endothelial progenitor cells and their different contributions to neovascularogenesis. *Arterioscler Thromb Vasc Biol* 2004; 24(2): 288–293.
- Meruane MA, Rojas M and Marcelain K. The use of adipose tissue-derived stem cells within a dermal substitute improves skin regeneration by increasing neovascularization and collagen synthesis. *Plast Reconstr Surg* 2012; 130: 53–63.
- Formigli L, Paternostro F, Tani A, et al. MSCs seeded on bioengineered scaffolds improve skin wound healing in rats. *Wound Repair Regen* 2015; 23(1): 115–123.

5. Griffith CK, Miller C, Sainson RC, et al. Diffusion limits of an in vitro thick prevascularized tissue. *Tissue Eng* 2005; 11(1-2): 257–266.
6. Auger FA, Gibot L and Lacroix D. The pivotal role of vascularization in tissue engineering. *Annu Rev Biomed Eng* 2013; 15: 177–200.
7. Egana JT, Danner S, Kremer M, et al. The use of glandular-derived stem cells to improve vascularization in scaffold-mediated dermal regeneration. *Biomaterials* 2009; 30(30): 5918–5926.
8. Clayton ZE, Sadeghipour S and Patel S. Generating induced pluripotent stem cell derived endothelial cells and induced endothelial cells for cardiovascular disease modelling and therapeutic angiogenesis. *Int J Cardiol* 2015; 197: 116–122.
9. Später T, Frueh FS, Nickels RM, et al. Prevascularization of collagen-glycosaminoglycan scaffolds: stromal vascular fraction versus adipose tissue-derived microvascular fragments. *J Biol Eng* 2018; 12: 24.
10. Frueh FS, Später T, Lindenblatt N, et al. Adipose tissue-derived microvascular fragments improve vascularization, lymphangiogenesis, and integration of dermal skin substitutes. *J Invest Dermatol* 2017; 137(1): 217–227.
11. Laschke MW and Menger MD. The dorsal skinfold chamber: a versatile tool for preclinical research in tissue engineering and regenerative medicine. *Eur Cell Mater* 2016; 32: 202–215.
12. Reinke JM and Sorg H. Wound repair and regeneration. *Eur Surg Res* 2012; 49: 35–43.
13. Sunderkötter C, Steinbrink K, Goebeler M, et al. Macrophages and angiogenesis. *J Leukoc Biol* 1994; 55: 410–422.
14. Barrientos S, Stojadinovic O, Golinko MS, et al. Growth factors and cytokines in wound healing. *Wound Repair Regen* 2008; 16: 585–601.
15. Nucera S, Biziato D and De Palma M. The interplay between macrophages and angiogenesis in development, tissue injury and regeneration. *Int J Dev Biol* 2011; 55(4–5): 495–503.
16. Garash R, Bajpai A, Marcinkiewicz BM, et al. Drug delivery strategies to control macrophages for tissue repair and regeneration. *Exp Biol Med* 2016; 241(10): 1054–1063.
17. Später T, Körbel C, Frueh FS, et al. Seeding density is a crucial determinant for the in vivo vascularisation capacity of adipose tissue-derived microvascular fragments. *Eur Cell Mater* 2017; 34: 55–69.
18. Frueh FS, Später T, Scheuer C, et al. Isolation of murine adipose tissue-derived microvascular fragments as vascularization units for tissue engineering. *J Vis Exp* 2017; 122: 5721.
19. Später T, Frueh FS, Menger MD, et al. Potentials and limitations of Integra® flowable wound matrix seeded with adipose tissue-derived microvascular fragments. *Eur Cell Mater* 2017; 33: 268–278.
20. Hunter MM, Wang A, Parhar KS, et al. In vitro-derived alternatively activated macrophages reduce colonic inflammation in mice. *Gastroenterology* 2010; 138(4): 1395–1405.
21. Weisser SB, van Rooijen N and Sly LM. Depletion and reconstitution of macrophages in mice. *J Vis Exp* 2012; 66: 4105.
22. Später T, Frueh FS, Karschnia P, et al. Enoxaparin does not affect network formation of adipose tissue-derived microvascular fragments. *Wound Repair Regen* 2018; 26: 36–45.
23. Shepard N and Mitchell N. Simultaneous localization of proteoglycan by light and electron microscopy using toluidine blue O—A study of epiphyseal cartilage. *J Histochem Cytochem* 1976; 24(5): 621–629.
24. Grässer C, Scheuer C, Parakenings J, et al. Effects of macrophage-activating lipopeptide-2 (MALP-2) on the vascularisation of implanted polyurethane scaffolds seeded with microvascular fragments. *Eur Cell Mater* 2016; 32: 74–86.
25. Nakano M, Nakajima Y, Kudo S, et al. Effect of autotransplantation of microvessel fragments on experimental random-pattern flaps in the rat. *Eur Surg Res* 1998; 30(3): 149–160.
26. Stone R 2nd and Rathbone CR. Microvascular fragment transplantation improves rat dorsal skin flap survival. *Plast Reconstr Surg Glob Open* 2016; 4(12): e1140.
27. Nakano M, Nakajima Y, Kudo S, et al. Successful autotransplantation of microvessel fragments into the rat heart. *Eur Surg Res* 1999; 31(3): 240–248.
28. Shepherd BR, Hoying JB and Williams SK. Microvascular transplantation after acute myocardial infarction. *Tissue Eng* 2007; 13(12): 2871–2879.
29. Pilia M, McDaniel JS, Guda T, et al. Transplantation and perfusion of microvascular fragments in a rodent model of volumetric muscle loss injury. *Eur Cell Mater* 2014; 28: 11–23; discussion 23.
30. Orth M, Altmeyer MAB, Scheuer C, et al. Effects of locally applied adipose tissue-derived microvascular fragments by thermoresponsive hydrogel on bone healing. *Acta Biomater* 2018; 77: 201–211.
31. Ruehle MA, Li MA, Cheng A, et al. Decorin-supplemented collagen hydrogels for the co-delivery of bone morphogenetic protein-2 and microvascular fragments to a composite bone-muscle injury model with impaired vascularization. *Acta Biomater* 2019; 93: 210–221.
32. Später T, Frueh FS, Metzger W, et al. In vivo biocompatibility, vascularization, and incorporation of Integra® dermal regenerative template and flowable wound matrix. *J Biomed Mater Res B Appl Biomater* 2018; 106: 52–60.
33. van Rooijen N and van Kesteren-Hendriks E. “In vivo” depletion of macrophages by liposome-mediated “suicide.” *Methods Enzymol* 2003; 373: 3–16.
34. Van Rooijen N and Sanders A. Liposome mediated depletion of macrophages: mechanism of action, preparation of liposomes and applications. *J Immunol Methods* 1994; 174(1–2): 83–93.
35. Van Rooijen N and Sanders A. Kupffer cell depletion by liposome-delivered drugs: comparative activity of intracellular clodronate, propamidine, and ethylenediaminetetraacetic acid. *Hepatology* 1996; 23(5): 1239–1243.
36. Nakamura T, Abu-Dahab R, Menger MD, et al. Depletion of alveolar macrophages by clodronate-liposomes aggravates ischemia-reperfusion injury of the lung. *J Heart Lung Transplant* 2005; 24(1): 38–45.
37. Schmidt-Weber CB, Rittig M, Buchner E, et al. Apoptotic cell death in activated monocytes following incorporation of clodronate-liposomes. *J Leukoc Biol* 1996; 60: 230–244.
38. Fink K, Ng C, Nkenfou C, et al. Depletion of macrophages in mice results in higher dengue virus titers and highlights the role of macrophages for virus control. *Eur J Immunol* 2009; 39(10): 2809–2821.

39. Kameka AM, Haddadi S, Jamaldeen FJ, et al. Clodronate treatment significantly depletes macrophages in chickens. *Can J Vet Res* 2014; 78(4): 274–282.
40. Ferenbach DA, Sheldrake TA, Dhaliwal K, et al. Macrophage/monocyte depletion by clodronate, but not diphtheria toxin, improves renal ischemia/reperfusion injury in mice. *Kidney Int* 2012; 82: 928–933.
41. Vignery A. Macrophage fusion: the making of osteoclasts and giant cells. *J Exp Med* 2005; 202(3): 337–340.
42. Walshe TE. TGF-beta and microvessel homeostasis. *Microvasc Res* 2010; 80(1): 166–173.
43. Moore EM and West JL. Harnessing macrophages for vascularization in tissue engineering. *Ann Biomed Eng* 2019; 47(2): 354–365.
44. Blau HM and Banfi A. The well-tempered vessel. *Nat Med* 2001; 7(5): 532–534.
45. Jetten N, Verbruggen S, Gijbels MJ, et al. Anti-inflammatory M2, but not pro-inflammatory M1 macrophages promote angiogenesis in vivo. *Angiogenesis* 2014; 17: 109–118.
46. DiPietro LA. Wound healing: the role of the macrophage and other immune cells. *Shock* 1995; 4(4): 233–240.
47. Rymo SF, Gerhardt H, Wolfhagen Sand F, et al. A two-way communication between microglial cells and angiogenic sprouts regulates angiogenesis in aortic ring cultures. *PLoS One* 2011; 6(1): e15846.
48. Khalil N, Bereznay O, Sporn M, et al. Macrophage production of transforming growth factor beta and fibroblast collagen synthesis in chronic pulmonary inflammation. *J Exp Med* 1989; 170(3): 727–737.
49. Hirschi KK, Rohovsky SA and D'Amore PA. PDGF, TGF-beta, and heterotypic cell-cell interactions mediate endothelial cell-induced recruitment of 10T1/2 cells and their differentiation to a smooth muscle fate. *J Cell Biol* 1998; 141(3): 805–814.
50. Bjorkerud S. Effects of transforming growth factor-beta 1 on human arterial smooth muscle cells in vitro. *Arterioscler Thromb* 1991; 11(4): 892–902.
51. Kojima S, Harpel PC and Rifkin DB. Lipoprotein (a) inhibits the generation of transforming growth factor beta: an endogenous inhibitor of smooth muscle cell migration. *J Cell Biol* 1991; 113(6): 1439–1445.
52. Reynolds LE, Conti FJ, Lucas M, et al. Accelerated re-epithelialization in beta3-integrin-deficient mice is associated with enhanced TGF-beta1 signaling. *Nat Med* 2005; 11(2): 167–174.
53. Hunt TK, Knighton DR, Thakral KK, et al. Studies on inflammation and wound healing: angiogenesis and collagen synthesis stimulated in vivo by resident and activated wound macrophages. *Surgery* 1984; 96(1): 48–54.
54. Desnues B, Ihrig M, Raoult D, et al. Whipple's disease: a macrophage disease. *Clin Vaccine Immunol* 2006; 13: 170–178.
55. Ehrchen JM, Roth J and Barczyk-Kahlert K. More than suppression: glucocorticoid action on monocytes and macrophages. *Front Immunol* 2019; 10: 2028.